Membrane bending by protein phase separation

Authors: Feng Yuan[1], Haleh Alimohamadi[2], Brandon Bakka[1], Andrea N. Trementozzi[1], Nicolas L. Fawzi[3], Padmini Rangamani[2*], Jeanne C. Stachowiak[1,4,*]

[1]University of Texas at Austin, Department of Biomedical Engineering

[2]University of California San Diego, Department of Mechanical and Aerospace Engineering

[3]Brown University, The Robert J and Nancy D Carney Institute for Brain Science & Department of Molecular Pharmacology, Physiology and Biotechnology

[4]University of Texas at Austin, Institute for Cellular and Molecular Biosciences

**to whom correspondence should be addressed:* padmini.rangamani@eng.ucsd.edu, jcstach@austin.utexas.edu

Abstract

Membrane bending is a ubiquitous cellular process that is required for membrane traffic, cell motility, organelle biogenesis, and cell division. Proteins that bind to membranes using specific structural features, such as wedge-like amphipathic helices and crescent-shaped scaffolds, are thought to be the primary drivers of membrane bending. However, many membrane-binding proteins have substantial regions of intrinsic disorder, which lack a stable three-dimensional structure. Interestingly, many of these disordered domains have recently been found to form networks stabilized by weak, multi-valent contacts, leading to assembly of protein liquid phases on membrane surfaces. Here we ask how membrane-associated protein liquids impact membrane curvature. Using synthetic and cell-derived membrane vesicles, we find that liquid-liquid phase separation of membrane-associated disordered proteins creates a substantial compressive stress in the plane of the membrane. This stress drives the membrane to bend away from the protein layer, creating protein-lined membrane tubules. A simple mechanical model of this process accurately predicts the experimentally measured relationship between the rigidity of the membrane and the diameter of the membrane tubules. Discovery of this mechanism, which may be relevant to a broad range of membrane protrusions, illustrates that membrane remodeling is not exclusive to structured scaffolds, but can also be driven by the rapidly emerging class of liquid-like protein networks that assemble at membranes.

Introduction

From endocytic buds (1) to needle-like filopodial protrusions (2), membrane surfaces with radii of curvature below 100 nanometers play a critical role in many cellular processes

(3). The energetic cost of creating these highly curved surfaces is considerable, such that spontaneous membrane fluctuations are insufficient to establish and stabilize the shapes of cellular membranes (4). Instead, work during the past two decades has revealed that interactions between proteins and lipids drive membrane curvature (5). Multiple physical mechanisms underlie the ability of proteins to shape membrane surfaces. These include amphipathic helices that insert like wedges into one leaflet of the membrane, creating an inter-leaflet area mismatch that drives curvature (6). Alternatively, proteins with inherently curved membrane binding domains, such as BAR domains, dynamin, and ESCRTs, act as scaffolds that can stabilize curved membrane geometries (7, 8). While each of these mechanisms relies on structured protein domains, we have recently reported that intrinsically disordered proteins, which lack a stable three-dimensional structure, can also be potent drivers of membrane bending (9, 10). Specifically, when non-interacting disordered domains are crowded together in cellular structures, steric repulsion among them drives the membrane to buckle toward the bound proteins, taking on a curved shape.

Interestingly, rather than repelling one another, many disordered proteins have recently been found to assemble together via weak, multi-valent interactions, forming networks that have the physical properties of liquids (11). Notably, recent studies have suggested that liquid-liquid phase separation of membrane-bound proteins plays an important role in diverse cellular processes including nucleation of actin filaments (12), immunological signaling (13), and assembly of virions (14).

How might liquid-liquid phase separation of proteins at membrane surfaces impact membrane curvature? To address this question, we examined phase separation of the N-terminal low complexity domain of fused in sarcoma, FUS LC, on the surfaces of synthetic and cell-derived membrane vesicles. FUS LC was chosen as a model protein for this study because it is among the most thoroughly characterized examples of a domain that undergoes liquid-liquid protein phase separation in solution (15). Here, we assemble FUS LC on membrane surfaces using an N-terminal histidine tag (16) that binds strongly to lipids with Ni-NTA headgroups. As FUS LC accumulated at the membrane surface, we observed protein phase separation in the two-dimensional plane of the membrane, followed by spontaneous inward bending of the membrane, such that protein-lined tubules were created. Interestingly, these tubules frequently had an undulating morphology, similar to a string of pearls, a phenomenon that has been associated in the literature with an area mismatch between the two membrane leaflets (17, 18). This observation suggests that protein phase separation pulls lipid head groups toward one another, creating a compressive stress on one side of the membrane. In line with this hypothesis, a continuum mechanics model recreated the tubule morphology when a compressive stress was imposed on the outer membrane surface. Further, the model predicted that tubule diameter should increase with increasing membrane rigidity and increasing rigidity ratio, trends confirmed by our experiments. Collectively, these findings

suggest that protein phase separation on membrane surfaces generates considerable stresses that can drive the spontaneous assembly of membrane buds and tubules with physiologically relevant dimensions.

Results and Discussion

Protein phase separation on membranes drives assembly of protein-lined tubules.

To examine the impact of protein phase separation on membrane surfaces, we combined an N-terminal 6 histidine-tagged version of FUS LC, his-FUS LC, with giant unilamellar vesicles consisting of 93 mol% POPC, 5 mol% Ni-NTA, 2 mol% DP-EG10 biotin for coverslip tethering, and 0.1 mol% Texas Red-DHPE for visualization, Figure 1a. The protein was labeled at the N-terminus with an NHS-reactive dye, Atto 488 for visualization, as described under materials and methods. Samples were imaged using multi-channel, high magnification spinning disc confocal microscopy. When a protein concentration of 0.5 μM was applied to the vesicles, a relatively dim, uniform signal from the protein was observed at the membrane surface, Figure 1b. In contrast, when the protein concentration was increased to 1 μM, more intense regions of fluorescence in the protein channel were observed around the vesicle periphery, Figure 1c. Three dimensional reconstruction of image stacks revealed that these bright regions formed hemispherical domains on the vesicle surfaces, which were surrounded by dimmer regions, Figure 1c, protein panel.

The appearance of these vesicles is remarkably similar to vesicles undergoing phase separation into two coexisting lipid phases (19, 20). In particular, the protein-rich regions in Figure 1c,d have smooth, rounded boundaries, suggesting that they enclose an easily deformable liquid (19). However, the membrane composition used in the present study consisted entirely of unsaturated lipids with melting temperatures well below room temperature, such that phase separation of the underlying lipid membrane was not expected. Further, a control protein that is not involved in protein phase separation, histidine-tagged GFP, covered the surfaces of these vesicles uniformly, Figure S1. These results suggest that the variations in intensity in the his-FUS LC protein channel did not arise from lipid heterogeneity. Instead the FUS LC protein appeared to organize on the two-dimensional membrane surface into protein-rich and protein-poor phases. Notably, the head-labeled lipid probe, Texas Red DHPE, was slightly brighter within the protein-rich regions, likely owing to affinity between the aromatic fluorophore on the lipid headgroup and the FUS LC domain, which is enriched in aromatic tyrosine residues (15). Photophysical effects of FUS LC on Texas Red could also play a role. To separate the lipid label from FUS LC, we also conducted experiments with a tail group labeled lipid, Texas Red-ceramide. Here enrichment of the labeled lipid in the protein-rich regions was lost, Figure S2.

A few minutes after the addition of his-FUS LC, we observed that many of the vesicles developed lipid tubules spontaneously. These tubules originated at the surfaces of the vesicles and protruded into the vesicle lumen, such that they were lined by the his-FUS LC protein, Figure 1d. Some of the tubules had an undulating, wavy appearance, Figure 1d,e, while others formed a series of tight spheres, resembling a string of pearls, Figure 1f. Still others were so slender that their morphology could not be precisely determined, Figure 1g. For well resolved tubules, dynamic fluctuations in morphology were observed, suggesting that the protein layer on the membrane surface remained highly deformable, rather than assembling into a rigid scaffold, Figure 1i, Supplementary Movie 1.

Tubules were observed more frequently as the concentration of his-FUS LC increased. Specifically, less than 2% of vesicles formed lipid tubules in the presence of 0.1 μM FUS LC, while 22% and 44% formed tubules after addition of 0.5 μM and 1 μM FUS LC, respectively. However, for protein concentrations above 1 μM, the fraction of vesicles with tubules reached a plateau, likely owing to the appearance of three-dimensional protein-only droplets in the surrounding solution, which were not membrane associated, Fig. 1h (inset). These droplets likely compete with the membrane surface for protein molecules, limiting the further accumulation of protein on the membrane surface. To further quantify the relationship between protein concentration and tubule formation, we next varied the strength of protein-protein and protein-membrane interactions and observed the impact on the. membrane tubules.

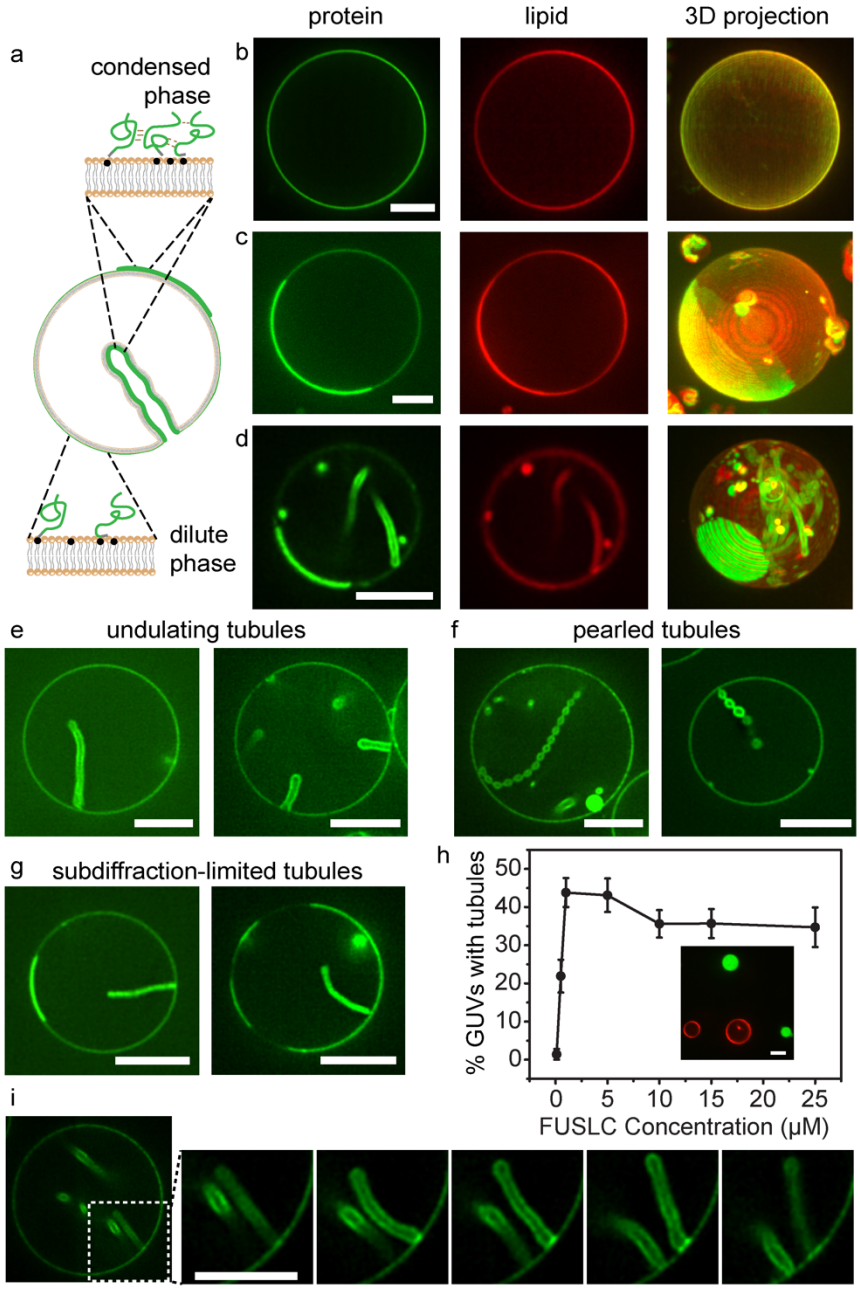

Figure 1. Protein phase separation on membranes drives assembly of protein-lined tubules. (**a**) Pictorial representation of his-FUS LC liquid-liquid protein phase separation on GUV membranes and inward tubule formation. Green lines represent FUS LC proteins. Grey domains indicated 6×his tags, and the black dots indicate Ni-NTA lipids. (**b-g)** Representative super-resolution images of GUVs incubated with 0.5 μM (**b**) and 1 μM atto-488 labeled his-FUS LC (**c-g**) in 25 mM HEPES, 150 mM NaCl buffer, pH 7.4. (**b-d**) Representative confocal images (lipid and protein channels) and corresponding maximum intensity projects of GUVs incubated with his-FUS LC. Some GUVs are covered uniformly by the protein (**b**), while others display 2D LLPS (**c**), which is frequently correlated with the formation

of lipid tubules (**d**). (**e-g)** Three kinds of membrane tubule structures were observed: undulating tubules (**e**), tubules consisting of a string of pearls (**f**), and sub-diffraction limited tubules, the structure of which cannot be clearly resolved (**g**). GUV membrane composition: 93 mol% POPC, 5 mol% Ni-NTA, 2 mol% DP-EG10 biotin and 0.1 mol% Texas Red-DHPE. (**h**) The fraction of GUVs displaying inward tubules as a function of his-FUS LC concentration. Data represent mean ± standard deviation; n = 3 independent experiments; N > 100 GUVs were acquired in each replicate. When the addition of his-FUS LC was greater than 5 μM, protein droplets were observed in the surrounding medium (inset in **h**). (**i**) Confocal image series illustrating dynamic fluctuations in tubule shape. All scale bars correspond to 5 μm.

Assembly of lipid tubules depends on the strength of protein-protein and protein-membrane interactions.

The membrane tubules in Figure 1 appear to emerge from the protein-rich regions of the membrane surface, suggesting that they rely on self-association of membrane-bound his-FUS LC molecules. We would expect that the ability of these proteins to come together on membrane surfaces depends on both the extent of protein-membrane binding and the strength of protein-protein interactions. Therefore, the assembly of membrane tubules likely depends upon these parameters. To vary the extent of protein-membrane binding, we varied the concentration of Ni-NTA-DOGS lipids in the membrane vesicles. To vary the strength of interactions between his-FUS LC proteins, we varied the concentration of sodium chloride in the solution. This approach is based on published studies showing that the saturation concentration for liquid-liquid phase separation of FUS LC decreases as sodium chloride concentration increases, resulting in enhanced phase separation (16).

Holding the concentration of his-FUS LC constant at 1 μM, we mapped the prevalence of two-dimensional protein phase separation and lipid tubules as a function of both NaCl concentration (50 mM – 250 mM) and the concentration of Ni-NTA-DOGS lipids (2-15 mol%), Figure 2a-d. We observed that increasing either parameter led to an increase in both the fraction of vesicles exhibiting phase separation, Figure 2e, and the fraction of vesicles exhibiting lipid tubules, Figure 2f. Specifically, only 5% of vesicles containing 2% Ni-NTA DOGS exhibited phase separation when the NaCl concentration was 50 mM, Figure 2e. This fraction increased to 22% as NaCl concentration increased to 250 mM, but no tubules were observed, Figure 2e. In contrast, a substantial fraction of vesicles containing 15% Ni-NTA DOGS exhibited phase separation and tubule formation at all NaCl concentrations, Figure 2b,e,f. Intermediate between these extremes, vesicles containing 5% Ni-NTA DOGS transitioned from infrequent to frequent incidence of both phase separation and tubule formation as the concentration of NaCl increased, Figure 2c-f. Plotting the fraction of phase separated vesicles versus the fraction of vesicles with lipid tubules, reveals a sharp transition to strong tubule formation when approximately

25% or more of the vesicles display phase separation, Figure 2g, Pearson's correlation coefficient, 0.8.

These results demonstrate that formation of protein-lined lipid tubules is strongly correlated with phase separation of his-FUS LC on membrane surfaces. However, it remains unclear why phase separation on membrane surfaces drives the membrane to bend inward, toward the lumen of the vesicle. In order to understand this phenomenon, we developed a continuum mechanical model of membrane bending in the presence of protein phase separation.

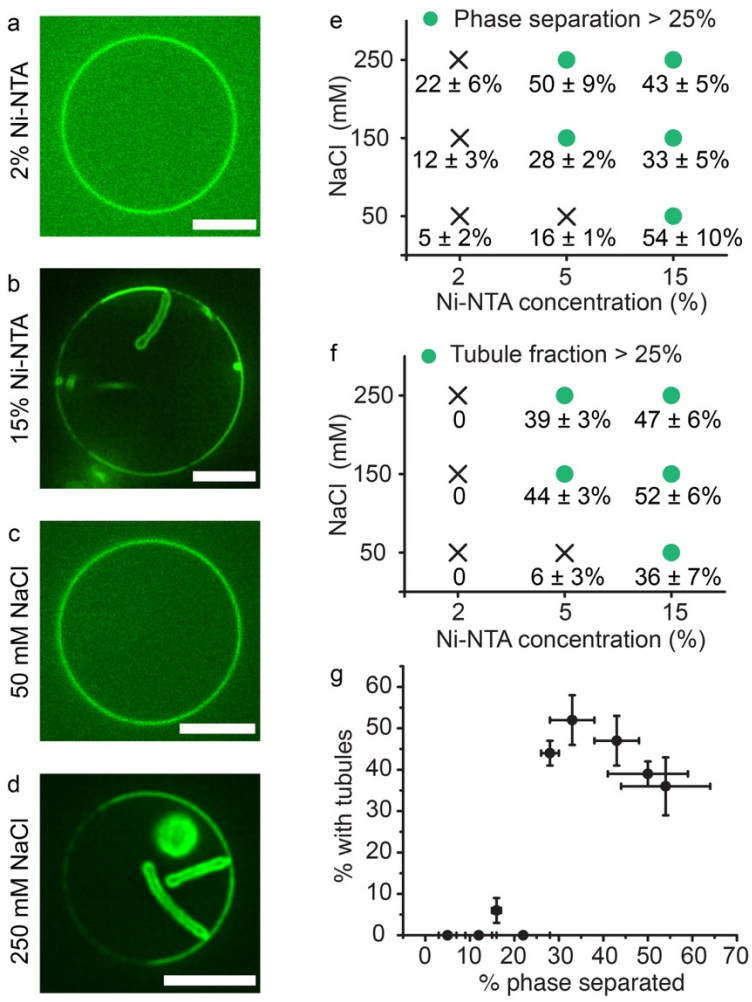

Figure 2. Protein phase separation and tubule formation depend upon the concentration of membrane-bound proteins and the strength of protein-protein interactions . (**a**) Representative confocal images of FUS LC bound to GUVs (composition: 96 mol% POPC, 2 mol% Ni-NTA, 2 mol% DP-EG10-biotin, 0.1 mol% Texas Red-DHPE) containing 2% Ni-NTA, and (**b**) GUVs (composition: 83 mol% POPC, 15 mol% Ni-NTA, 2 mol% DP-EG10-biotin, 0.1 mol% Texas Red-

DHPE) containing 15% Ni-NTA. GUVs were incubated with 1μM Atto-488 labeled his-FUS LC in 25 mM HEPES, 150 mM NaCl pH 7.4 buffer. (**c, d**) Representative images of GUVs (93 mol% POPC, 5 mol% Ni-NTA, 2 mol% DP-EG10 biotin and 0.1 mol% Texas Red-DHPE made in 560 mOsmo glucose solution) incubated with 1μM atto-488 labeled FUS LC in 25 mM HEPES pH 7.4 buffer containing (**c**) 50 mM and (**d**) 250 mM NaCl, respectively. Glucose was added to the buffers accordingly to maintain osmotic pressure balance. All scale bars represent 5 μm. (**e, f**) Percentage of GUVs displaying inward (**e**) lipid tubules and (**f**) protein phase separation as a function of Ni-NTA content, and NaCl concentration. Green dots indicate fractions exceeding 25%. (**g**) Percentage of GUVs with inward tubules as a function of percentage of GUVs with phase separation. Here the Pearson's correlation coefficient between phase separation and tubule formation was 0.8. Data are shown as mean value ± standard deviation. N > 100 GUVs were analyzed cumulatively from three independent replicates for each condition.

A continuum mechanics model predicts tubule shape and dependence of tubule diameter on membrane bending rigidity.

The morphologies of the tubules that we have observed can provide insights into the mechanism by which protein phase separation drives membrane bending. Some tubules consist of a well-defined "string of pearls" in which spherical shapes are separated by thin necks, Figures 1f. Other tubules have an undulating morphology in which the "pearls" are less well defined, with some tubules being nearly cylindrical, Figure 1e, 2b,d. This set of shapes - pearls, undulations, and cylinders - can be classified as Delaunay surfaces (21), which have a constant, non-zero mean curvature, Figure 3a. This class of surfaces encompass cylinders and unduloids. Unduloids are surfaces of revolution of an elliptic catenary (21, 22). With small changes in geometric parameters, a range of unduloid surfaces can be constructed (21), Figure 3a. More importantly, Delaunay surfaces, particularly unduloids and their variants, are known to minimize the Helfrich energy for membrane bending (22). The radius and shape of the unduloids depends on a single dimensionless parameter $\alpha = \sqrt{\frac{\lambda}{2\kappa C_0^2} + \frac{1}{4}}$, where λ is the membrane tension, κ is the bending modulus, and C_0 is the spontaneous curvature. When $\alpha = 0.75$, the membrane resembles a cylinder and for $\alpha > 0.75$, the membrane resembles an unduloid, Figure 3a.

Tubules with unduloid-like morphologies are known to arise when there is an area mismatch between the inner and outer leaflets of the lipid bilayer, such that the membrane has a finite spontaneous curvature (23). For example, addition of lipids (17), polymers (24), and proteins (25) to the surfaces of membrane vesicles have each been shown to produce such tubules. However, in these cases, the tubules protruded outward from the membrane surfaces, as would be expected when the area of the outer leaflet exceeds that of the inner leaflet. In contrast, we observed tubules that protrude inward from the

membrane surface, suggesting that protein phase separation reduces the area of the outer leaflet relative to that of the inner leaflet, Figure 3b. We might expect such a reduction in area if phase separation of his-FUS LC pulls lipid headgroups together, creating compressive forces in the outer membrane leaflet that increase the local density of lipids.

To examine this idea we developed a model in which a compressive stress is applied to one leaflet of a lipid bilayer. The membrane bending energy was modeled using the Helfrich framework (26). The area difference between the two leaflets was modeled using a locally specified spontaneous curvature for simplicity in simulations, Figure 3c. See the supplemental information for detailed model assumptions and derivations. The spontaneous curvature effectively represents the stresses due to the area difference between the two leaflets (27). The governing equations were solved in an axisymmetric parametrization for ease of computation to demonstrate the principles underlying the formation of undulated and pearled tubules.

We simulated a domain of fixed area and homogeneous bending rigidity that included the protein enriched phase and the surrounding protein depleted phase. Our results show that increasing the spontaneous curvature in the protein-rich phase resulted in the formation of undulated tubules, Figure 3d, similar to those observed in experiments, Figure 1. Furthermore, the simulations predicted that the tubule diameter would increase linearly in proportion to the square root of the bending modulus, Figure 3e. The bending energy corresponding to the formation of the undulated and pearled tubules is shown in Figure S3.

Thus far, we have assumed that the membrane has a uniform bending rigidity in the protein enriched and protein depleted phases. However, it is likely that the protein enriched phase has an increased bending rigidity compared to the protein depleted phase, owing to the higher density of protein contacts. Therefore, we asked if the ratio of bending rigidities in the attached protein layer and the underlying membrane layer could impact the tube diameter. We defined the ratio of bending rigidities, $\kappa_{ratio} = \frac{\kappa_{protein}}{\kappa_{membrane}}$, and varied the ratio in the range of 1-20, where $\kappa_{ratio} = 1$ denotes uniform bending rigidity. With increasing κ_{ratio}, we observed that the tubules took on a more clearly-defined pearled morphology, Figure 3f and Figure S4, similar to those observed in some of our experiments, Figure 1f. Here our simulations predict that the diameter of the tubules will increase linearly in proportion to the square root of κ_{ratio}, Figure 3g. We next sought to test the predictions of these simulations with experimental data.

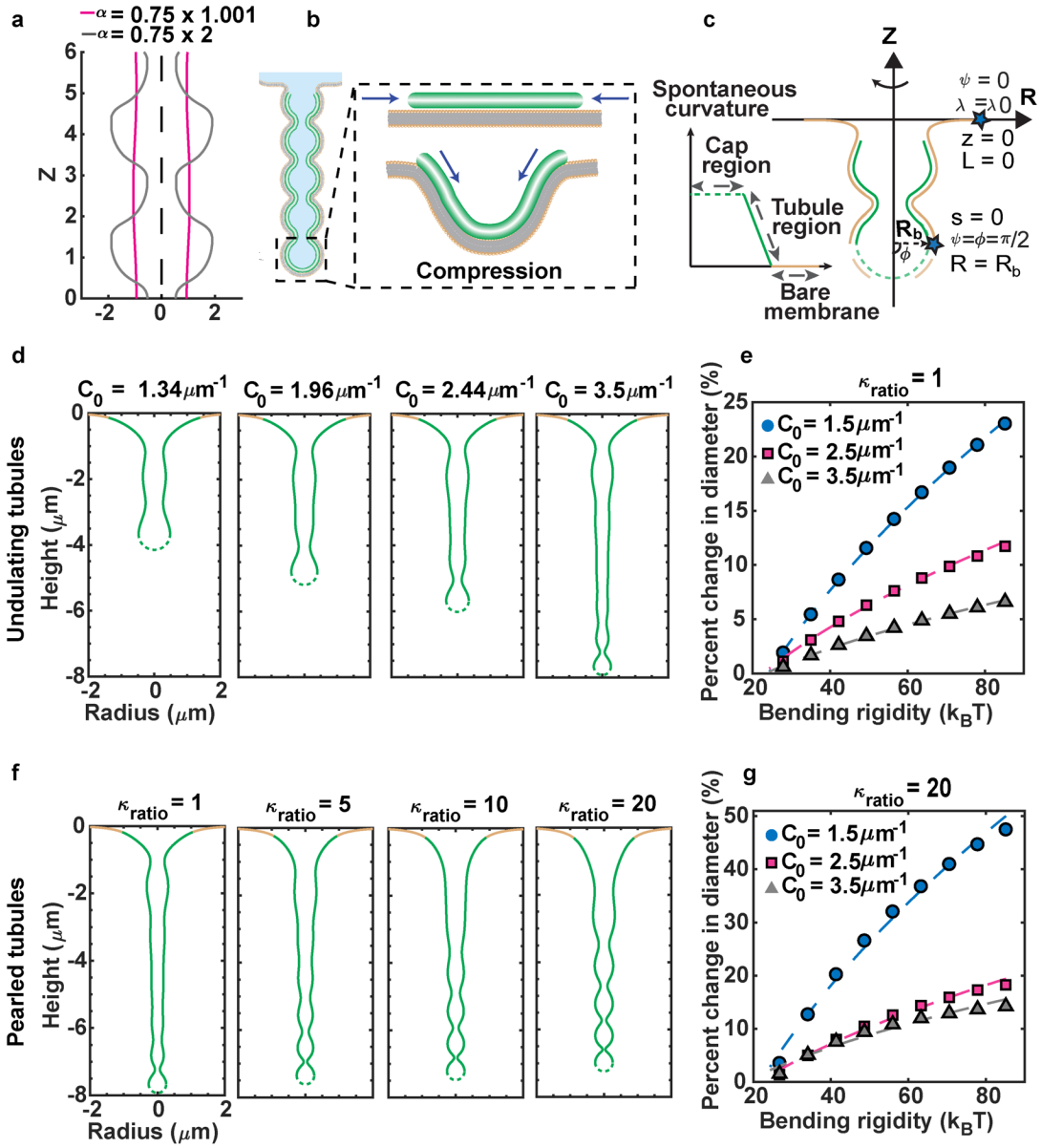

Figure 3. Mechanical model of undulated and pearled tubule formation. (**a**) Unduloid-like shapes solution for Helfrich energy minimization at different values of non-dimensional parameter,α. For α~ 0.75, the membrane takes on a cylindrical shape (purple line); for α> 0.75, the unduloid becomes a sphere similar to a string of pearls (gray line). (**b**) Schematic depiction of membrane tubule formation due to the induced compressive stresses from the phase-separated protein domain. (**c**) Schematic of the axisymmetric simulations depicting the simulation domain and the boundary conditions. The yellow region represents the bare membrane and the green region is the coated area by the proteins. The dashed lines indicate the cap of the tubule, assumed to have a constant curvature. The inset shows the spontaneous curvature distribution along the tubule region used to model the membrane shape. (**d**) Undulated tubules minimize the membrane bending energy as the spontaneous curvature increase for uniform bending rigidity of the

membrane (κ = 80 k_BT). (**e**) Percentage of change in the tubule diameter (($D-D_{\kappa = 25\ kBT}$)/$D_{\kappa = 25\ kBT}$) as a function of the bending rigidity for three different values of spontaneous curvature. The dashed lines show a square root dependence on the bending modulus by fitting to the curve ($A\sqrt{\kappa} + B$) where for the gray line A=5.4, B=-26.44; for the pink line A= 2.71, B=-12.9; and for the blue line, A=1.53 and B=-7.4. (**f**) Pearled tubules minimize the bending energy of the membrane for heterogeneous membrane rigidity (κ_{ratio}= $\kappa_{protein-domain}/\kappa_{bare\ membrane}$), C_0 = 3.5 μm^{-1}. (**g**) Percentage of change in the tubule diameter (($D-D_{\kappa = 25\ kBT}$)/$D_{\kappa = 25\ kBT}$) as a function of the bending rigidity for three different values of spontaneous curvature for κ_{ratio}= 20 . The dashed lines are the fitted curve ($A\sqrt{\kappa} + B$) where for the gray line; A=10.98, B=-51.31, for the pink line; A= 4.22, B=-19.58, and for the blue line; A=3.1 and B=-13.

Tubule diameter varies with membrane bending rigidity and salt concentration.

Our continuum model predicted that the radii of the tubules should increase in proportion to the square root of the membrane bending rigidity. To examine this prediction, we measured the diameter of the lipid tubules formed by assembly of his-FUS LC on membrane surfaces, as a function of membrane bending rigidity, Figure 4a-e. As membrane bending rigidity was increased from approximately 20 k_BT to approximately 76 k_BT, through variations in membrane lipid composition, we observed a substantial increase in membrane tubule diameter from 240 ± 120 nm (S. E.) to 420 ± 280 nm (S. E.), Figure 4e. For each lipid composition, tubules with both pearled and undulating morphologies were observed, Figure 4a-d. Further, the data were reasonably well fit by a curve in which tubule diameter was proportional to bending rigidity, in agreement with the predictions of the simulation, compare Figure 4f, Figure 3e,g. Here optical reassignment during spinning disc confocal microscopy, followed by deconvolution was used to increase the optical resolution to better than 150 nm (28).

A second prediction from our simulation is that the tubule diameter should increase as the rigidity of the protein-rich phase increases, while the rigidity of the underlying membrane is held constant. To test this prediction, we examined the impact of sodium chloride concentration on tubule diameter. Increasing sodium chloride concentration has been previously shown to increase the strength of interactions between FUS LC molecules in condensed phases (15). Therefore, we inferred that his-FUS LC might assemble into a denser, more rigid protein layer at high salt concentration.

As the sodium chloride concentration increased from 50 mM to 250 mM, we observed an increase in tubule diameter of approximately 75%, from 240 ± 20 nm to 420 ± 40 nm, in qualitative agreement with simulation results, compare Figure 4g with Figure 3g. Further, the incidence of tightly pearled tubules increased significantly as NaCl concentration increased from 50 mM to 250 mM, in agreement with simulations, Figure 4h. A constant osmotic pressure was maintained in all experiments, see methods. Collectively these data

suggest that protein phase separation applies a compressive stress to the membrane surface, resulting in assembly of protein tubules directed inward from the membrane surface.

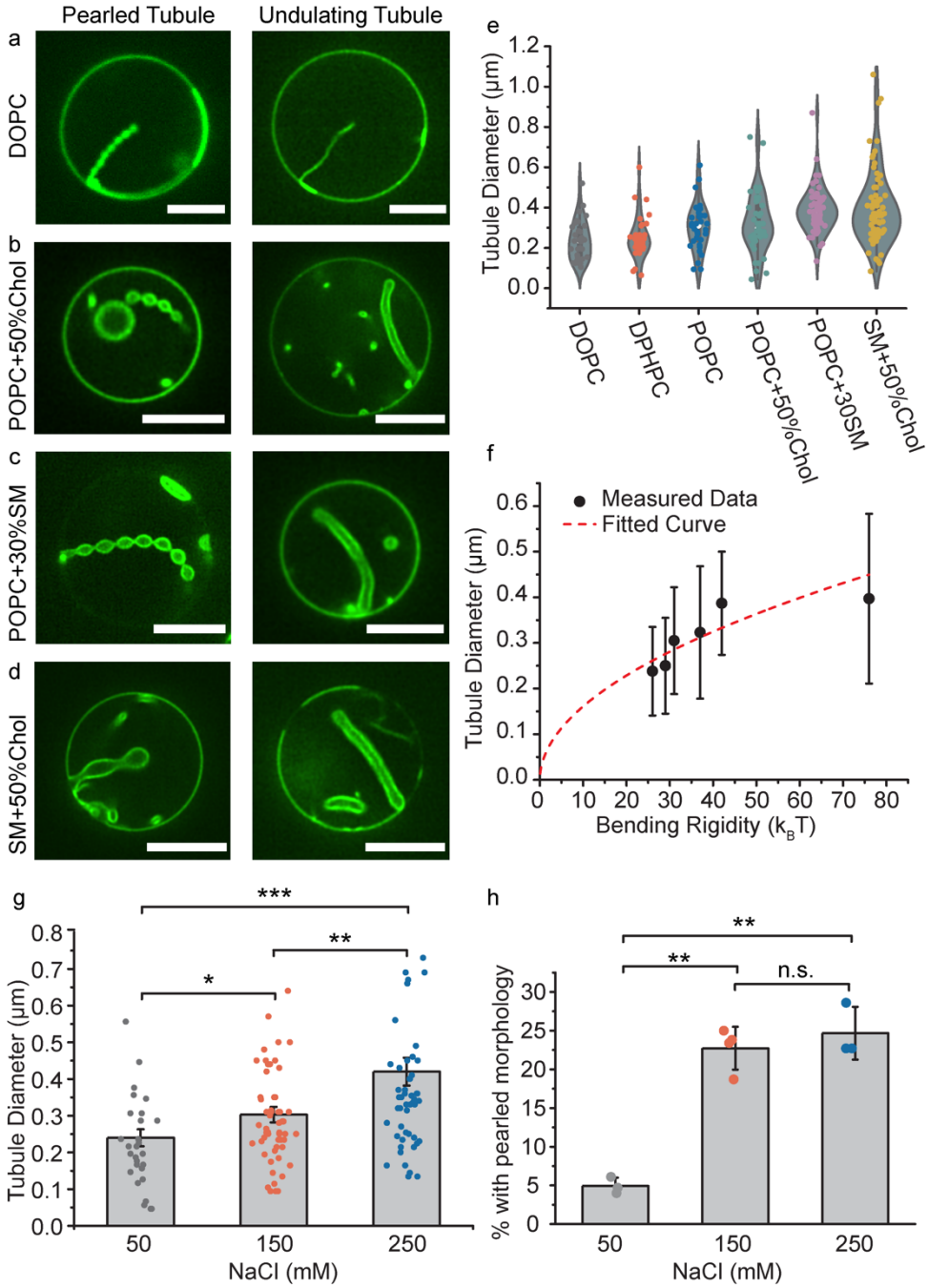

Figure 4. Tubule diameter varies with membrane bending rigidity and salt concentration. (**a-f**) Six groups of GUVs with different compositions (listed in Table 1 in Materials and Methods) were used to vary membrane bending rigidity. GUVs were incubated with 1μM atto-488 labeled his-FUS LC in 25 mM HEPES, 150 mM NaCl pH 7.4 buffer. (**a-d**) Representative super-resolution confocal

images tubules with pearled (left panel) and undulating morphologies (right panel), from GUVs consisting primarily of (**a**) DOPC, (**b**) POPC + 50% Chol, (**c**) POPC + 30% SM, and (**d**) SM + 50% Chol. All scale bars are 5 μm. (**e)** Violin plot showing the measured tubule diameter distribution for each membrane GUV composition group. (**f)** GUV tubule diameter as a function of membrane bending rigidity. Data points from left to right represent DOPC, DPHPC, POPC, POPC + 50% Chol, POPC + 30% SM, and SM + 50% Chol, respectively. Data are displayed as mean ± standard deviation from three independent experiments (n = 3) on separate preparations of vesicles, with cumulatively N > 100 vesicles categorized for each composition. The measured tubule diameters increase roughly as the square root of membrane bending rigidity (red dash line, R^2 = 0.78). (**g**) Bar chart displaying average tubule diameter under different NaCl concentrations. GUVs (composition: 83 mol% POPC, 15 mol% Ni-NTA, 2 mol% DP-EG10-biotin and 0.1% Texas Red-DHPE) were incubated with 1μM atto-488 labeled his-FUS LC in 25 mM HEPES, pH 7.4 buffer with corresponding NaCl concentration under iso-osmotic conditions. Error bars correspond to standard deviation. Each point is a mean value of diameters measured at three positions along the same tubule. N > 100 GUVs were acquired cumulatively from three independent replicates for each condition. (**h**) Fraction of tubules that displayed a pearled morphology as a function of NaCl concentration Data are displayed as mean ± standard deviation from three independent experiments (n = 3) on separate preparations of vesicles, with cumulatively N > 100 vesicles categorized. Brackets show statistically significant comparisons using an unpaired, 2-tailed student's t test. * represents $p < 0.05$, ** represents $p < 0.01$, *** represents $p < 0.001$, and n.s. indicates a difference that was not statistically significant.

Protein phase separation drives tubule formation from cell-derived membranes.

While our present experiments rely on synthetic interactions between lipids and a model protein, it is interesting to consider whether protein phase separation at membrane surfaces is sufficient to drive remodeling of cellular membranes. To address this question, we derived membrane vesicles from the plasma membranes of mammalian retinal pigment epithelial, RPE, cells. To facilitate binding of FUS LC to the surfaces of these vesicles, we engineered the donor cells to express a chimeric transmembrane protein that consisted of the transmembrane domain of the transferrin receptor, fused to an extracellular blue fluorescing protein, BFP, domain for visualization. This chimera displayed a nanobody against GFP on the cell surface, Fig. 5a,b. Membrane blebs extracted from these cells also displayed the nanobody on their surfaces, which facilitated the recruitment of GFP-tagged proteins, Fig. 5a,b. Adding soluble GFP domains to the solution surrounding these blebs resulted in GFP being strongly concentrated at the bleb surfaces, Fig. 5c. Notably, the GFP signal appeared to separate into brighter and dimmer regions on the surfaces of some of the blebs. This separation within blebs has been

observed previously (29), and is thought to arise from lipid phase separation, in which the transferrin receptor transmembrane domain is known to prefer the liquid disordered membrane phase (30).

When a GFP-tagged version of FUS LC, GFP-FUS LC (31), was introduced to blebs taken from the same donor cells, the GFP signal was similarly concentrated at the bleb surfaces, Figure 5d. However, the surfaces of blebs exposed to GFP-FUS LC did not remain flat. Instead, regions of the bleb surfaces with intense GFP signal bent inward, creating inwardly directed, protein-lined membrane buds and tubules. Many of the tubules had pearl-like and undulating morphologies, similar to tubules formed by exposure of synthetic vesicles to his-FUS LC, compare Figures 1 and 5d. The diameter of the tubules ranged broadly from 150 nm to more than 1 μm, Figure 5e. Here, the average tubule diameter, 570 ± 260 nm (S. D.), which was somewhat larger than that of tubules formed from synthetic membranes. This difference could arise from the enhanced bending rigidity of cell-derived membranes, which contain a high density of transmembrane proteins. Alternatively, the GFP-FUS LC protein, which has been observed to form gel-like assemblies in solution (31, 32), may increase the rigidity of the protein layer. However, the range of curvatures observed in these cell-derived vesicles encompasses that of many cellular structures including filopodia, dendritic spines, phagosomes, and many organelles (3).

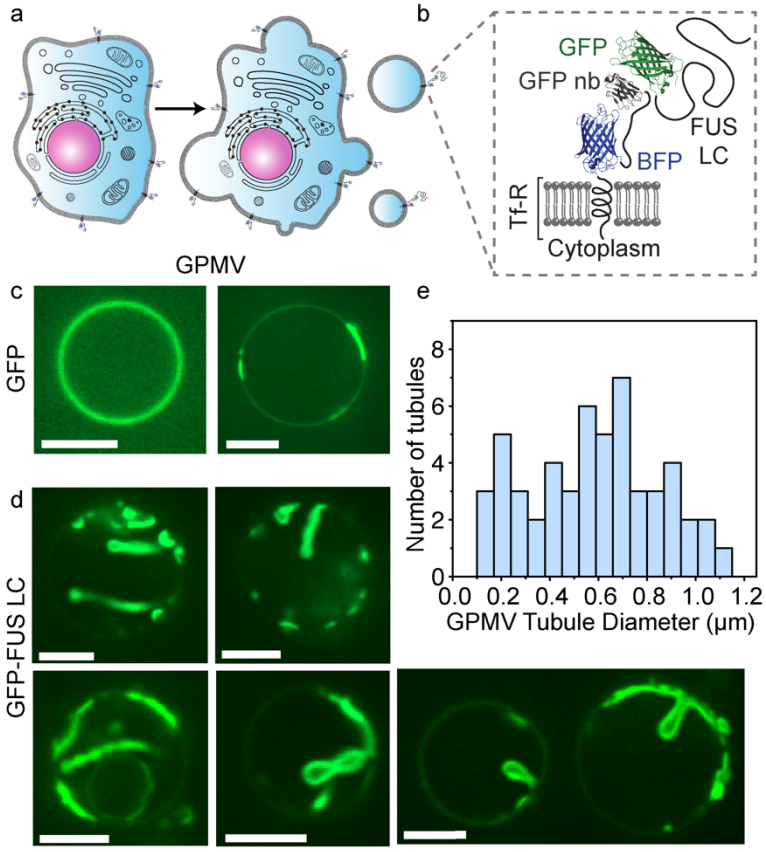

Figure 5. Protein phase separation can drive tubule formation from cell-derived membranes. (**a**) Cartoon showing extraction of giant plasma membrane vesicles (GPMVs) from donor RPE cells. (**b**) Schematic of the architecture of the membrane receptor and ligand protein. GFP-FUS LC is recruited to the GPMV membrane by binding to a GFP nanobody displayed on the cell surface. (**c)** Confocal images of GPMVs incubated with 2 μM GFP and (**d**) GFP-FUS LC in buffer containing 10 mM HEPES, 2 mM $CaCl_2$, 150 mM NaCl, pH 7.4 . Scale bar = 5 μm. (**e**) Distribution of diameters of tubules formed from GPMVs. N= 50 tubules measured.

Conclusions

Here, we demonstrate that protein phase separation at membrane surfaces can drive the assembly of protein-lined membrane tubules of physiologically relevant dimensions. This mechanism of membrane remodeling is physically distinct from known mechanisms. In particular, protein assemblies previously found to drive membrane curvature have consisted of solid scaffolds, which include the rigid, helical assemblies of BAR domains and dynamin rings, as well as the precise cage-like geometries of protein coats formed by clathrin, COPII, and many viral capsids (7, 33, 34). In contrast, we show that a model protein that forms liquid-like assemblies (15) can drive the formation of membrane tubules with dynamic cylindrical and unduloid morphologies, Figure 1, Supplementary Movie 1. These results illustrate that increasing the spontaneous curvature of a membrane, which is the fundamental requirement for membrane bending (4), is not exclusive to structured scaffolds, but can also arise from liquid-like protein interactions that generate stresses at membrane surfaces. Using this mechanism, cytosolic proteins that phase separate at membrane surfaces could contribute to outward membrane protrusions such as filopodia, dendritic spines, viral buds, and cilia. In contrast, proteins and receptors that assemble on the outer cell surface could contribute to structures that bud into the cell, such as endocytic vesicles.

What advantage might a liquid scaffold offer for membrane remodeling? We speculate that the lower energy barriers to assembly and disassembly associated with a liquid may allow the membrane greater freedom to deform into a variety of shapes and dimensions, rather than the more narrowly defined set of geometries observed for most structured scaffolds. Indeed many curved membrane structures from cytoskeletal protrusions (35) to the endoplasmic reticulum (36), are known to have heterogenous and dynamic morphologies. In light of the ongoing discovery of liquid-like behavior in many membrane-bound protein networks (37), the ability of protein phase separation to shape membranes has the potential to impact diverse membrane-associated processes throughout the cell.

Acknowledgements

This research was supported by the National Institutes of Health through grants R01GM112065 to J.C.S., R01GM132106 to P.R., and R01GM118530 to N.L.F F and by the Human Frontiers Science Program to N.L.F. RGP0045/2018. The plasmid DNA for GFP FUS LC was provided by the lab of S. McKnight, UTSW.

References

1. Kirchhausen T, Owen D, & Harrison SC (2014) Molecular structure, function, and dynamics of clathrin-mediated membrane traffic. *Cold Spring Harb Perspect Biol* 6(5):a016725.
2. Mattila PK & Lappalainen P (2008) Filopodia: molecular architecture and cellular functions. *Nat Rev Mol Cell Biol* 9(6):446-454.
3. Hurley JH, Boura E, Carlson L-A, & Różycki B (2010) Membrane budding. *Cell* 143(6):875-887.
4. Zimmerberg J & Kozlov MM (2006) How proteins produce cellular membrane curvature. *Nature reviews. Molecular cell biology* 7(1):9-19.
5. Stachowiak JC, Brodsky FM, & Miller EA (2013) A cost-benefit analysis of the physical mechanisms of membrane curvature. *Nature Cell Biology* 15(9):1019-1027.
6. Drin G & Antonny B (2010) Amphipathic helices and membrane curvature. *FEBS letters* 584(9):1840-1847.
7. Daumke O, Roux A, & Haucke V (2014) BAR domain scaffolds in dynamin-mediated membrane fission. *Cell* 156(5):882-892.
8. Christ L, Raiborg C, Wenzel EM, Campsteijn C, & Stenmark H (2017) Cellular Functions and Molecular Mechanisms of the ESCRT Membrane-Scission Machinery. *Trends Biochem Sci* 42(1):42-56.
9. Busch DJ, Houser JR, Hayden CC, Sherman MB, Lafer EM, & Stachowiak JC (2015) Intrinsically disordered proteins drive membrane curvature. *Nature Communications* 6:7875.
10. Snead WT, Zeno WF, Kago G, Perkins RW, Richter JB, Zhao C, Lafer EM, & Stachowiak JC (2019) BAR scaffolds drive membrane fission by crowding disordered domains. *J Cell Biol* 218(2):664-682.
11. Brangwynne Clifford P, Tompa P, & Pappu Rohit V (2015) Polymer physics of intracellular phase transitions. *Nature Physics* 11:899.
12. Banjade S & Rosen MK (2014) Phase transitions of multivalent proteins can promote clustering of membrane receptors. *Elife* 3.

13. Huang WYC, Alvarez S, Kondo Y, Lee YK, Chung JK, Lam HYM, Biswas KH, Kuriyan J, & Groves JT (2019) A molecular assembly phase transition and kinetic proofreading modulate Ras activation by SOS. *Science* 363(6431):1098-1103.

14. Alenquer M, Vale-Costa S, Etibor TA, Ferreira F, Sousa AL, & Amorim MJ (2019) Influenza A virus ribonucleoproteins form liquid organelles at endoplasmic reticulum exit sites. *Nat Commun* 10(1):1629.

15. Burke KA, Janke AM, Rhine CL, & Fawzi NL (2015) Residue-by-Residue View of In Vitro FUS Granules that Bind the C-Terminal Domain of RNA Polymerase II. *Mol Cell* 60(2):231-241.

16. Murthy AC, Dignon GL, Kan Y, Zerze GH, Parekh SH, Mittal J, & Fawzi NL (2019) Molecular interactions underlying liquid-liquid phase separation of the FUS low-complexity domain. *Nat Struct Mol Biol* 26(7):637-648.

17. Sanborn J, Oglecka K, Kraut R, & Parikh A (2013) Transient pearling and vesiculation of membrane tubes under osmotic gradients. *Faraday Discussions* 161:167-176.

18. Tsafrir I, Sagi D, Arzi T, Guedeau-Boudeville M, Frette V, Kandel D, & Stavans J (2001) Pearling instabilities of membrane tubes with anchored polymers. *Phys. Rev. Lett.* 86(6):1138-1141.

19. Veatch SL & Keller SL (2003) Separation of liquid phases in giant vesicles of ternary mixtures of phospholipids and cholesterol. *Biophys. J.* 85(5):3074-3083.

20. Baumgart T, Hess ST, & Webb WW (2003) Imaging coexisting fluid domains in biomembrane models coupling curvature and line tension. *Nature* 425(6960):821-824.

21. Kreyszig E (1959) *Differential geometry* (University of Toronto Press, Toronto,) pp xiv, 352 p.

22. Naito H, Okuda M, & Zhongcan OY (1995) New Solutions to the Helfrich Variation Problem for the Shapes of Lipid Bilayer Vesicles - Beyond Delaunays Surfaces. *Phys. Rev. Lett.* 74(21):4345-4348.

23. Bar-Ziv R & Moses E (1994) Instability and pearling states produced in tubular membranes by competition of curvature and tension. *Phys. Rev. Lett.* 73(10):1392-1395.

24. Tsafrir I, Sagi D, Arzi T, Guedeau-Boudeville MA, Frette V, Kandel D, & Stavans J (2001) Pearling instabilities of membrane tubes with anchored polymers. *Phys. Rev. Lett.* 86(6):1138-1141.

25. Snead WT, Hayden CC, Gadok AK, Zhao C, Lafer EM, Rangamani P, & Stachowiak JC (2017) Membrane fission by protein crowding. *Proc Natl Acad Sci U S A* 114(16):E3258-E3267.

26. Helfrich W (1973) Elastic Properties of Lipid Bilayers - Theory and Possible Experiments. *Zeitschrift Fur Naturforschung C-a Journal of Biosciences* C 28(11-1):693-703.

27. Wiese W, Harbich W, & Helfrich W (1992) Budding of Lipid Bilayer Vesicles and Flat Membranes. *J Phys-Condens Mat* 4(7):1647-1657.

28. Hayashi S (2016) Resolution doubling using confocal microscopy via analogy with structured illumination microscopy. *Jpn J Appl Phys* 55(8).

29. Lorent JH, Diaz-Rohrer B, Lin XB, Spring K, Gorfe AA, Levental KR, & Levental I (2018) Structural determinants and functional consequences of protein affinity for membrane rafts (2017). *Nature Communications* 9.

30. Harder T, Scheiffele P, Verkade P, & Simons K (1998) Lipid domain structure of the plasma membrane revealed by patching of membrane components. *Journal of Cell Biology* 141(4):929-942.

31. Kato M, Han TNW, Xie SH, Shi K, Du XL, Wu LC, Mirzaei H, Goldsmith EJ, Longgood J, Pei JM, Grishin NV, Frantz DE, Schneider JW, Chen S, Li L, Sawaya MR, Eisenberg D, Tycko R, & McKnight SL (2012) Cell-free Formation of RNA Granules: Low Complexity Sequence Domains Form Dynamic Fibers within Hydrogels. *Cell* 149(4):753-767.

32. Murray DT, Kato M, Lin Y, Thurber KR, Hung I, McKnight SL, & Tycko R (2017) Structure of FUS Protein Fibrils and Its Relevance to Self-Assembly and Phase Separation of Low-Complexity Domains. *Cell* 171(3):615-627 e616.

33. Faini M, Beck R, Wieland FT, & Briggs JA (2013) Vesicle coats: structure, function, and general principles of assembly. *Trends Cell Biol* 23(6):279-288.

34. Luque D & Caston JR (2020) Cryo-electron microscopy for the study of virus assembly. *Nat Chem Biol* 16(3):231-239.

35. Ridley AJ (2011) Life at the Leading Edge. *Cell* 145(7):1012-1022.

36. Pendin D, McNew JA, & Daga A (2011) Balancing ER dynamics: shaping, bending, severing, and mending membranes. *Current Opinion in Cell Biology* 23(4):435-442.

37. Snead WT & Gladfelter AS (2019) The Control Centers of Biomolecular Phase Separation: How Membrane Surfaces, PTMs, and Active Processes Regulate Condensation. *Mol Cell* 76(2):295-305.